Torsions, low-frequency vibrations and vibration-torsion ("vibtor") levels in the *m*-chlorotoluene cation

David J. Kemp, Lewis G. Warner and Timothy G. Wright[a]

School of Chemistry, University of Nottingham, University Park, Nottingham NG7 2RD, UK

[a] Tim.Wright@nottingham.ac.uk

ABSTRACT

Zero-electron-kinetic-energy (ZEKE) spectra are presented for *m*-chlorotoluene (*m*ClT), employing different low-lying torsional and vibration-torsional ("vibtor") levels of the S_1 state as intermediates. The adiabatic ionization energy (AIE) is determined to be 71319 ± 5 cm^{-1} (8.8424 ± 0.0006 eV). It is found that the activity in the ZEKE spectra varies greatly for different levels and is consistent with the assignments of the S_1 levels of *m*-fluorotoluene (*m*FT) deduced in the recent fluorescence study of Stewart et al. [J. Chem. Phys. **150**, 174303 (2019)] and the ZEKE study from Kemp et al. [J. Chem. Phys. **151**, 084311 (2019)]. As with *m*FT, the intensities in the ZEKE spectra of *m*ClT are consistent with a phase change in the torsional potential upon ionization, allowing large number of torsions and vibtor levels to be observed for the cation. Vibration-induced modifications of the torsional potential are discussed. Calculated vibrational wavenumbers for the S_0, S_1 and D_0^+ states are also presented.

I. INTRODUCTION

Energy flow in molecules is now generally accepted as being facilitated by the coupling of both methyl torsion and vibrational motions and so is important for understanding the photophysics of molecules.[1,2] A very recent example highlights the role vibrational excitation has in light harvesting.[3] Understanding the processes occurring in complicated molecules is greatly aided by detailed studies on small molecules, and recent examples from our, the Reid and Lawrance groups have looked at toluene,[4,5,6] *para*-fluorotoluene (*p*FT)[7,8,9,10,11,12,13,14,15] and *para*-xylene (*p*Xyl),[10,16,17] using a combination of fluorescence and photoionization spectroscopies. These studies have elucidated how vibration-vibration and vibration-torsion coupling can drive the transition to statistical ("dissipative") intramolecular vibrational redistribution (IVR), underpinning energy dispersal and photostability.[10,12]

Timbers et al.[18] have concluded that *meta*-fluorotoluene (*m*FT) undergoes IVR more than an order of magnitude faster than *p*FT, showing that the location of substituents is likely to be important in the coupling. Recently, Stewart et al.[19] have examined the first 350 cm^{-1} of the $S_1 \leftarrow S_0$ transition of *m*FT, assigning the spectra with the use of two-dimensional laser-induced fluorescence (2D-LIF), and in a follow-up study[20] we studied the same S_1 energy levels using ZEKE spectroscopy. The spectra were assigned in terms of torsional and vibration-torsional ("vibtor") levels in the S_0, S_1 and D_0^+ states.

Stewart et al.[19] concluded that there are interactions between the torsional motion and low frequency vibrations in both the S_0 and S_1 states of *m*FT and postulated that such interactions may be present in the cation. In Ref. 20 we confirmed the latter suggestion, and highlighted that in the cation the torsional potential was being altered by the vibrational motion. In the present work, we wish to explore whether the same interactions occur in *m*-chlorotoluene (*m*ClT). Of course, vibrational wavenumbers may alter with a different substituent and this is likely to affect vibtor interactions. The present work on *m*ClT builds upon the work of Ichimura et al.,[21] who recorded laser-induced fluorescence (LIF) and dispersed fluorescence (DF) spectra, and of Feldgus et al.[22] who have reported a resonance-enhanced multiphoton ionization (REMPI) spectrum and zero-electron-kinetic-energy (ZEKE) spectra via a handful of the lowest-wavenumber S_1 levels.

II. EXPERIMENTAL

The REMPI/ZEKE apparatus employed was the same as that used in earlier work.[23] The focused, frequency-doubled outputs of two dye lasers (Sirah CobraStretch) were overlapped spatially and temporally, and passed through a vacuum chamber coaxially and counterpropagating, where they intersected a free jet expansion of *m*ClT (Alfa Aesar, 98% purity) in 1.5 bar Ar. The sample container and nozzle were heated to ~50ºC to obtain a high enough vapour pressure to give a strong signal. The excitation laser operated with Coumarin 540A and was pumped with the third harmonic (355 nm) of a Surelite III Nd:YAG laser, while the ionization laser operated with Pyrromethene 597, pumped with the second harmonic (532 nm) of a Surelite I Nd:YAG laser. All spectra presented in the present work were recorded in the ^{35}Cl isotopologue mass channel, although spectra were also recorded separately in the ^{37}Cl isotopologue mass channel, but no significant shifts were seen over the spectral range scanned herein.

The jet expansion passed between two biased electrical grids located in the extraction region of a time-of-flight mass spectrometer, which was employed in the REMPI experiments. These grids were also used in the ZEKE experiments by application of pulsed voltages, giving typical fields of ~10 V cm^{-1}, after a delay of up to 2 μs; this delay was minimized while avoiding the introduction of excess noise from the prompt electron signal. The resulting ZEKE bands had widths of ~5-7 cm^{-1}. Electron and ion signals were recorded on separate sets of microchannel plates.

III. RESULTS AND ASSIGNMENTS

A. Nomenclature and labelling

1. Vibrational and Torsional Labelling

We employ the D_i labels from Ref. 24 for the vibrations of *m*ClT as used in the recent work by Stewart et al.[19] and ourselves for *m*FT[20] – see Table I. This C_s point group labelling scheme[24] is based on the vibrations of the *meta*-difluorobenzene (*m*DFB) molecule, developed to be applicable to both symmetric and asymmetric substitutions. We note that Ichimura et al.[21] employed Wilson labels in their jet-cooled fluorescence study, which do not describe the motions very well;[24] therefore, in Table I, we have "translated" these into the D_i labels for both the S_0 and S_1 states. It may be seen that the gas phase DF values[21] for the S_0 state agree well with earlier infrared and Raman values (discussed in depth in Ref. 24). Both the DF and LIF values for the S_0 and S_1 states are in good agreement with the calculated values.

Since the G_6 molecular symmetry group (MSG) is appropriate for vibtor levels in *m*ClT, we shall use these symmetry labels throughout. In addition, torsional levels will be labelled via their *m* quantum number – see Refs. 16 or 19. The correspondence between the C_s point group labels and the G_6 MSG ones is given in Table II. To calculate the overall symmetry of a vibtor level, it is necessary to use the corresponding G_6 label for the

vibration, and then find the direct product with the symmetry of the torsion (Table II), noting that a C_{3v} point group direct product table can be used, since the G_6 MSG and the C_{3v} point group are isomorphic.

Under the free-jet expansion conditions employed here, almost all of the molecules are expected to be cooled to their zero-point vibrational level, and thus essentially all $S_1 \leftarrow S_0$ pure vibrational excitations are expected to be from this level. In contrast, owing to nuclear-spin and rotational symmetry,[16] the molecules can be in one of either the $m = 0$ or $m = 1$ torsional levels in the S_0 state.

2. Transitions and Coupling

When designating excitation transitions, we shall generally omit the lower level, since it will be obvious from the jet-cooled conditions. In the usual way, vibrational transitions will be indicated by the cardinal number, i, of the D_i vibration, followed by a super-/subscript specifying the number of quanta in the upper/lower states, respectively; torsional transitions will be indicated by m followed by its value. Finally, vibtor transitions will be indicated by a combination of the vibrational and torsional transition labels (see Ref. 20, and below, for specific examples).

As has become common usage, we will generally refer to a level using the notation of a transition, with the level indicated by the specified quantum numbers, with superscripts indicating levels in the S_1 state and, when required, subscripts indicating levels in the S_0 state. Since we will also be referring to transitions and levels for the ground state cation, D_0^+, we shall indicate those as superscripts in the text, but with an additional single preceding superscripted + sign. (These signs are omitted in the figures for clarity.) Relative wavenumbers of the levels will be given with respect to the $m = 0$ zero-point vibrational level in each electronic state. (Again, see Ref. 20, and below, for specific examples.)

For cases where the geometry and the torsional potential are both similar in the S_1 and D_0^+ states, the most intense transition is expected to be that for which no changes in the torsional and/or vibrational quantum numbers occur: these will be designated as $\Delta m = 0$, $\Delta v = 0$ or $\Delta(v, m) = 0$ transitions, as appropriate. However, as will be seen, and as was reported for mFT,[20] the $\Delta m = 0$ and $\Delta(v, m) = 0$ transitions are almost always not the most intense bands in the ZEKE spectra, suggesting a significant change in the torsional potential upon ionization.

If two levels are close in wavenumber and have the same overall symmetry, then (except between vibrational fundamentals, to first order) interactions can occur, with the simplest example being the anharmonic interaction between two vibrational levels – the classic Fermi resonance.[25] For molecules that contain a hindered internal rotor then, if vibration-torsional coupling is present, interactions can also involve torsional or "vibtor" levels. The end result of such interactions is the formation of eigenstates with mixed character. Such couplings are only expected to be significant for small changes, $\Delta v \approx 3$, of the vibrational quantum

number, and also for changes, Δm, of 0, ±3 or ±6 in the torsional quantum number in descending order of likely strength.[26,27] Often the eigenstates will be referred to by the dominant contribution, with the context implying if an admixture is present.

3. Torsional energies

The energy levels of a hindered methyl rotor have been the subject of numerous studies, with the paper by Spangler[28] being a good starting point. For a hindered methyl rotor, the lowest couple of terms of the torsional potential may be expressed as:

$$V(\alpha) = \frac{V_3}{2}(1 - cos3\alpha) + \frac{V_6}{2}(1 - cos6\alpha) \quad (1)$$

where α is the torsional angle. If the V_6 term is small relative to V_3, which is usually the case, then its effect is simply to modify the shape of the potential. Recent work[22] has deduced that for *m*ClT, V_3 has approximate values of: 2 cm^{-1} for the S_0 state; 110 cm^{-1} for the S_1 state; and -285 cm^{-1} for the D_0^+ state. (The sign of the V_3 parameter is a way of indicating the phase of the torsional potential, and does not affect the energy levels, but it can be deduced from the calculated geometry.[29,30]) Thus, these three states of the same molecule are, respectively: very close to a free rotor; a moderately-hindered rotor; and a highly-hindered rotor.

In Ref. 20, we illustrated how the magnitude of the V_3 term affected the energies of the *m* levels for *m*FT. As described in Spangler,[28] as V_3 increases, deep within the potential well the free-rotor *m* levels evolve into triply degenerate torsional vibrations, with each torsional vibration arising from one degenerate pair of $m \neq 3n$ levels, plus one $m = 3n$ level. These latter levels lose their degeneracy in V_{3n} potentials and the resulting levels can be denoted $m = 3n(+)$ and $m = 3n(-)$, with the former being of a_1 and the latter of a_2 symmetry in G_6.[19,28] Thus, if the torsional barrier is high, we expect low-lying *e* symmetry levels to be close-to-degenerate with an $m = 3n(+)$ or $m = 3n(-)$ level. The splitting between the $m = 3n(+)$ and $m = 3n(-)$ levels is largely an effect of V_3, but is also affected by (the smaller-valued) V_6.[20] Although for a G_{12} symmetry molecule such as toluene or *p*FT, the sign of V_6 determines the energy ordering of the $m = 3n(+)$ and $m = 3n(-)$ levels, particularly for $n = 1$. For a G_6 symmetry molecule, the energies of the *m* levels depend on both parameters, as well as the effective rotational constant for torsion of the -CH_3 group, denoted *F*, whose value is expected to be only slightly different in the three electronic states under consideration. As a consequence, it is not straightforward to deduce the values of the torsional parameters from the spectrum directly, and that difficulty is further exacerbated by possible interactions between torsional, vibtor and vibrational levels.[19]

B. Spectra and assignments

1. Overview of the $S_1 \leftarrow S_0$ spectrum

The REMPI spectrum covering the first 350 cm^{-1} of the *m*ClT $S_1 \leftarrow S_0$ spectrum is shown in Figure 1; the assignments shown have been deduced in this work. Also shown is a comparison with the 0–350 cm^{-1} region of *m*FT, with assignments given for the latter that have been discussed recently.[19,20] As may be seen, these low-wavenumber regions consist of a series of bands that can be associated with torsions, vibtor and low-frequency vibrational levels. A laser-induced fluorescence (LIF) spectrum has been presented in Ref. 21 that shows transitions up to 1000 cm^{-1} above the origin, although assignments are only given for some of the bands up to 860 cm^{-1}. The calculated wavenumbers for the D_i vibrations of the S_0, S_1 and D_0^+ states are given in Table 1. In the present work, we shall make use of these quantum chemical calculations and the activity seen in the ZEKE spectrum, to deduce assignments in both the S_1 and D_0^+ states, and will comment on the previous *m*ClT assignments and values given in Refs. 21 and 22.

We note particularly that a number of the REMPI bands appear as doublets – see Figure 1. This attribute of the spectra arises from the population of both the m = 0 and m = 1 levels in the S_0 state owing to nuclear spin symmetry.[16] The lower wavenumber band is assigned to the m_1^1 transition, so that for the first intense doublet band in the spectrum, the true origin is the second of those two bands, which corresponds to the m_0^0 transition. Symmetry-allowed transitions from m = 1 in the S_0 state will be to S_1 levels of *e* symmetry, while those from m = 0 will be to those of a_1 symmetry, so that we expect very different ZEKE activity from these two levels.

2. Torsional levels

In Figure 2 and Figure 3, we show the ZEKE spectra recorded via the torsional levels of the S_1 state, separating these into a_1 and *e* symmetry, respectively. For the a_1 symmetry levels, we record spectra via m^0 and $m^{3(+)}$, while for the *e* levels we record spectra via the m^1, m^2 and m^4 levels. In contrast to *m*FT, we were unable to record spectra via the $m^{3(-)}$ and m^5 levels. As with *m*FT, we could record spectra via m = 2 accessed via both the m_1^2 and m_2^2 transitions, with the activity looking similar, but with the former having the better signal to noise, and so is the one presented herein.

In Figure 2, the ZEKE spectra via the a_1 symmetry m levels, m^0 and $m^{3(+)}$ are presented; the low wavenumber regions of these are similar to the spectra reported by Feldgus et al.,[22] although the current spectra span a wider range. It may immediately be seen that the most intense transition does not correspond to Δm = 0, but to $|\Delta m|$ = 3 in both cases. In the case of m = 0, the intensity of the ${}^+m^{6(+)}$ band is also sizeable. These are consistent with a change in phase of the torsional potential upon ionization, as seen for *m*FT.[20] Alongside the ${}^+m^{3(+)}$ and ${}^+m^{6(+)}$ are the symmetry-forbidden ${}^+m^{3(-)}$ and ${}^+m^{6(-)}$ bands, respectively; the activities of these could arise from rotation-torsion coupling[19,20] or vibronic/intrachannel coupling.[20]

We also see the symmetry-allowed $^{+}30^{1}m^{3(-)}$ band when ionizing via m^0, which was also seen for *m*FT.[20] To higher wavenumber, vibtor combinations involving $^{+}18^{1}$ and $^{+}19^{1}$ can be seen, with largely the same relative intensities as the lower wavenumber bands. These observations are very similar to those in our previous work on *m*FT,[20] except that only combinations with $^{+}18^{1}$ were observed. This could suggest that there are slightly different geometry changes upon ionization between the *m*FT and *m*ClT molecules, or that there is different Duschinsky mixing of the vibrations – this is the subject of ongoing work.

The $^{+}m^0$ band can be used to determine the adiabatic ionization energy (AIE), which is derived as 71319 ± 5 cm^{-1}. This value is slightly lower than the value of 71333 ± 5 cm^{-1} deduced by Feldgus et al.,[22] which we assume has been increased to reflect the lowering of the AIE by the applied electric field. However, we do not apply such a correction since the forced ionization of Rydberg states would lead to a very wide ZEKE band of ~ 15 cm^{-1}, with the actual AIE towards the high wavenumber end of the band. This is because of the well-known decay of the lower-lying Rydberg states accessed in the pulsed-field ionization process,[31] and this is confirmed by the fact that the ZEKE bands had widths of ~5-7 cm^{-1}, some of which is due to unresolved rotational structure.

In Figure 3 the ZEKE spectra recorded via three *e* symmetry levels, m^1, m^2 and m^4 are presented. The low wavenumber sections of those recorded via m^1 and m^2 are similar to the spectra reported by Feldgus et al.,[22] but the range here is larger; the spectrum recorded via m^4 is reported here for the first time. Across these three spectra, again, it is clear that the most intense transitions correspond to $|\Delta m| = 3$, rather than $\Delta m = 0$. Also, combinations with $^{+}18^{1}$ and $^{+}19^{1}$ are seen to higher wavenumber in all cases. Looking first at the ZEKE spectrum recorded via m^1, it can be seen that the $\Delta m = 3$ transitions to $^{+}m^2$ and $^{+}m^4$ (remembering that the m quantum number is signed for $m \neq 3n$) are intense; however, the transition to $^{+}m^5$ is also very intense, which is a $\Delta m = 6$ transition (in the case of *m*FT,[20] this was the most intense band). We also observe the $^{+}m^7$ band ($\Delta m = 6$) and the $^{+}m^8$ band ($\Delta m = 9$).

Of note is the strong activity of $^{+}30^{1}m^2$ when exciting via m^1. This band is so strong that Feldgus et al.[22] understandably suggested that there was a Fermi resonance between $^{+}m^5$ and $^{+}30^{1}m^2$. However, the relative intensities of the two corresponding bands when exciting via different intermediate levels (see Figure 3 and Section III.B.3) does not seem to support this. Rather, it appears that there is an anomalously strong transition intensity associated with the $^{+}30^{1}m^2 \leftarrow m^1$ ionization. This is analogous to the strong intensity of the $^{+}30^{1}m^4 \leftarrow m^4$ transition seen in the case of *m*FT.[20] In that work, we did see vibtor transitions associated with $^{+}30^{1}$ when exciting via m^1; however, these were relatively weak compared to the main $^{+}m^x$ bands; certainly the $^{+}30^{1}m^2$ band was significantly weaker than in the present case.

When exciting via m^2, there are strong transitions to $^{+}m^1$ ($\Delta m = 3$), $^{+}m^4$ ($\Delta m = 6$) and, to a lesser extent, $^{+}m^5$ ($\Delta m = 3$). Notably, the relative intensity of the $^{+}30^{1}m^2$ band seems to be significantly less than when exciting

via m^1; indeed, this also seems to be the case when exciting via m^4. In contrast, the $^+30^1m^4$ band is very intense when exciting via m^4, and this behaviour is similar to that observed for *m*FT,[20] although the $^+30^1m^5$ transition is much stronger for *m*ClT here. The ZEKE spectrum via m^4 is compared to the spectra obtained via m^1 and m^2. It can be seen that the $^+m^1$ band is intense, while the expected $^+m^7$ band is overlapped (both $|\Delta m|$ = 3). The $|\Delta m|$ = 6 band, $^+m^2$ is also intense. We show the same spectrum again in Figure 4, where its activity is compared to the spectra obtained via 30^1m^x vibtor levels (see Section III.B.3).

3. Vibtor levels involving 30^1

In Figure 4 we show the ZEKE spectra recorded via 30^1m^1, 30^1m^4 (overlapped with 30^2m^1), and $30^1m^{3(-)}$, and compare to the spectrum obtained via m^4 (also shown in Figure 3, where it is compared to ZEKE spectra recorded by other *e* symmetry torsional levels).

We note that the 30^1m^1 and m^4 transitions are relatively close to each other and are each of *e* symmetry; as such, there is the possibility of interaction between these two levels. The ZEKE spectrum via the former level is of the second trace in Figure 4, where it can be compared with that via m^4 (top trace). (The appearance of the 30^1m^1 ZEKE spectrum is clearly that of an m = 1 level.) It can be seen that there is a significant amount of cross-activity between the two spectra. This is of interest as it is not clear where the transition strength for the 30^1m^1 level originates. The usual vibronic interaction for substituted benzenes in the S_1 state would involve in-plane vibrations that are of a_1 symmetry, while the D_{30} vibration is an out-of-plane vibration of a_2 symmetry. Despite the weakness of the $^+30^1m^4$ band, which might be expected to be stronger, the appearance of the 30^1m^1 ZEKE spectrum is suggestive of a $m^4 \ldots 30^1m^1$ interaction in the S_1 state. The absence of nearby levels of a_2 symmetry to interact with it, and the absence of the corresponding 30^1m^0 band, supports an interaction of 30^1m^1 with an *e* symmetry torsional level.

The ZEKE spectrum recorded via the REMPI band at 206 cm^{-1} has significant activity in $^+30^1m^x$ and $^+30^2m^x$ bands. This leads to the deduction that it arises from two overlapped transitions, 30^1m^4 and 30^2m^1. The picture is slightly complicated by the strong $^+30^2m^4$ band observed when exciting via 30^1m^4 and the strong $^+30^1m^5$ band seen when exciting via 30^2m^1 in *m*FT,[20]. Similar activity is seen here via the 206 cm^{-1} band but, given the unusual intensities noted for *m*FT, it is difficult to state confidently which transitions have dominant contributions from 30^1m^4 or 30^2m^1, as it is likely that most transitions have contributions from both. Further comment on the 30^2m^1 contributions will be given in Section III.B.5

The appearance of the spectrum via $30^1m^{3(-)}$ is reminiscent of the corresponding and related spectra recorded for *m*FT,[20] with a strong Δm = 0 band and a significant $|\Delta m|$ = 3 band, although the $^+30^1m^0$ was not clearly visible here.

4. The band at 192 cm^{-1}

In Figure 5, we show the ZEKE spectrum recorded via the REMPI transition at 192 cm^{-1} above the origin. This spectrum is a little puzzling since if the first band is situated at 0 cm^{-1}, then the resulting cation internal wavenumber scale is not consistent with a number of the band positions; however, if some of their band positions are moved up by ~5 cm^{-1}, then many of these bands can be clearly assigned. We conclude that this spectrum consists of two sets of transitions, one involving a_1 symmetry levels and one *e* symmetry (the latter will be on an energy scale that differs by the $m = 1 - m = 0$ energy spacing in the S_0 state). As such, the REMPI band must be an overlap of two features: one involving levels of a_1 symmetry, commencing at the S_0 $m = 0$ level, and one involving levels of *e* symmetry, originating from the S_0 $m = 1$ level. The first band is seen to arise from the $^{+}m^0$ transition, with the $^{+}m^1$ transition being too weak to see definitively. A perusal of the possible S_1 levels that could give rise to these two overlapped features suggests one is 29^1m^2 and the other is $29^1m^{3(-)}$. Thus, the main bands arise from $^{+}29^1m^x$ transitions, of both a_1 and *e* symmetry. The wavenumber, and additionally since we do not expect the $\Delta(v,m) = 0$ band to be the most intense, indicates that it is more prudent to assign the most intense band at 273 cm^{-1} to $^{+}29^1m^{3(-)}$, with a contribution from $^{+}29^1m^2$. This is consistent with the feature at 173–178 cm^{-1} being an overlap of $^{+}29^1m^0$ and $^{+}29^1m^1$ contributions. Further, the band at ~455 cm^{-1} can be assigned as the $\Delta m = 3$ transition, $^{+}29^1m^{6(-)}$. A band at ~239 cm^{-1} seems most sensibly assignable to $^{+}30^1m^{3(-)}$, the bands at 300 cm^{-1} and 321 cm^{-1} to $^{+}m^{6(+)}$ and $29^130^1m^0$, respectively

That these REMPI bands overlap means that at least one of them must be subject to an interaction in the S_1 state. In fact, the 29^1m^2 level is expected close to 199 cm^{-1}, while the $29^1m^{3(-)}$ level is expected at about 207 cm^{-1}. Possible interactions involving these levels are $29^1m^{3(-)}\ldots30^2m^0$ and $29^1m^2\ldots30^2m^1$ which would provide some explanation for the larger-than-expected separation between 30^2m^0 and 30^2m^1 – see Section III.B.5; notwithstanding the lack of cross activity in the respective spectra. It is seen that the ZEKE band at ~300 cm^{-1} is slightly too high in wavenumber to be assigned to a $^{+}30^2$ band to support this; an alternative is that this ZEKE band is $^{+}m^{6(+)}$, and so indicative of a $29^1m^{3(-)}\ldots m^{6(+)}$ interaction, which would imply the unperturbed $m^{6(+)}$ level lies above $29^1m^{3(-)}$. We do not see a $m^{6(+)}$ band in the REMPI spectrum, so cannot confirm this hypothesis, although it seems reasonable. It is clear that there are a number of possible interactions involving the 29^1m^2 and $29^1m^{3(-)}$ levels.

5. Vibtor levels involving 30^2

ZEKE spectra recorded via the bands at 206 cm and 213 cm are shown in Figure 6. The REMPI band at 213 cm^{-1} is straightforwardly assigned to 30^2m^0 on the basis of its ZEKE spectrum, in particular the strong $^{+}30^2m^{3(+)}$ band. It is interesting that there is activity in several vibtor bands involving $^{+}21^1$, which was also the case for *m*FT.[20] We have noted above, that a distinct 30^2m^1 REMPI band was not observed for *m*ClT, but that it is believed this is overlapped by the 30^1m^4 transition (see Figure 4 and Section III.B.3); that ZEKE spectrum is presented again in Figure 6 for completeness and more-facile comparison with that of 30^2m^0. The separation between 30^2m^1 and 30^2m^0 is ~ 7 cm^{-1}, which is greater than the ~4 cm^{-1} for the m^1 and m^0 bands, confirming

vibtor interactions are occurring for at least one of these levels, and in Section III.B.4 we have suggested this is possibly with $29^1m^{3(-)}$; a similarly larger-than-anticipated separation was seen for *m*FT,[19,20] although a specific interaction was not identified. We also find that there is no discernible activity for $^+21^1$ vibtor levels in the 30^2m^1 ZEKE spectrum, and indeed only very weak $^+21^1m^x$ bands were seen in the corresponding ZEKE spectrum for *m*FT.[20]

6. Vibtor levels involving 21^1

Much more straightforward are the pair of ZEKE spectra recorded for 21^1m^1 and 21^1m^0, Figure 7, where the vibtor activity is similar to that observed for the m^1 and m^0 levels. The $^+30^2m^{3(+)}$ vibtor band is seen, mirroring the $^+21m^x$ activity seen in the 30^2m^0 ZEKE spectrum (Section III.B.5), and consistent with observations for *m*FT.[20]

7. Vibtor levels involving 29^2

The pair of ZEKE spectra recorded for 29^2m^0 and 29^2m^1 contain activity that is largely as expected – see Figure 8. This confirms their assignment, but shows that the REMPI bands are in the reverse order to that expected, with the 29^2m^0 band lying *below* that of 29^2m^1; moreover, the higher-wavenumber band is broader than expected (see top trace in Figure 8). For the ZEKE spectrum recorded via 29^2m^1, there are the expected $^+29^2m^x$ *e* symmetry vibtor bands, but in addition $^+29^1m^1$, $^+29^1m^4$ and $^+29^1m^5$ bands (unexpectedly, however, there is no $^+29^1m^2$ band). The ordering of the REMPI bands, the $^+29^1m^x$ activity, the broader profile of the higher wavenumber band (more consistent with a higher, *e* symmetry *m* level), and the expected energies of vibtor levels suggests a $29^2m^1\ldots29^1m^5$ interaction. Although too weak to record a ZEKE spectrum to confirm its assignment, there is a weak REMPI band at 287 cm^{-1} that can reasonably be associated with the partner level from this interaction (see top trace in Figure 8). We thus conclude that this $29^2m^1\ldots29^1m^5$ interaction has led to a shift in the expected band ordering of the 29^2m^0 and 29^2m^1 pair.

C. Torsional Potentials

A full fit of the torsional and vibtor levels, including vibtor interactions, has not been carried out in this work, since the precision does not merit it. However, significant insight can be obtained from the band separations, and these are tabulated in Table III. We first note that for the pure torsional levels, we have calculated the energies of the *m* levels by varying the V_3 and V_6 parameters, to obtain reasonable agreement with the experimental observations. Our best values are +110 cm^{-1} for V_3 for the S_1 state,and -287.5 cm^{-1} for the cation. These are both close to the values reported by Feldgus et al.,[22] and indeed the present positions of the bands are in excellent agreement with those reported therein. (We fixed the V_6 and *F* values to those given by Feldgus et al.[22]) Because of the need to vary three parameters, and the neglect of vibtor interactions, these values should be viewed as merely reasonable estimates. That said, the V_3 parameters for *m*ClT seem to be

about 5 cm^{-1} and between 10 and 15 cm^{-1} lower than those for *m*FT, for the S_1 and D_0^+ states, respectively; i.e. the torsional motion is less hindered in *m*ClT than in *m*FT. We note that the sign of V_3 cannot be established from the spectrum, and comes from optimized geometries. In agreement with Feldgus et al.,[22] the calculated geometries position the methyl group in the *pseudo*-trans orientation in the S_0 and S_1 states, i.e. the in-plane methyl hydrogen points away from the chlorine substituent, and *pseudo*-cis in the D_0^+ state – see Figure 9. This confirms the change in phase of the torsional potential, consistent with the significant torsion and vibtor activity seen in the spectrum, and the observation that the $\Delta(v,m) = 0$ band is mostly not the most intense feature.

Taking into account experimental uncertainties in measuring band centres, Table IV indicates that several of the vibrations of the cation have vibtor levels that have about the same spacings as those built upon the torsional levels associated with the vibrational origin: $^+18^1$, 19^1, $^+21^1$, 29^1, $^+29^2$. On the other hand, those built upon $^+30^1$, $^+30^2$ appear to have potentials that are less hindered, since the spacings are less than those associated with the vibrational origin. A similar picture was seen for *m*FT,[19,20] where it was noted that the out-of-plane D_{30} vibration coupled to the torsional motion more effectively than did the (also out-of-plane) D_{29} vibration, in both the S_1 and D_0^+ states. It was also noted in Ref. 20 that the in-plane D_{18} and D_{21} vibrations did not appear to couple significantly with the torsional motion, and that also is consistent with the data in Table IV. (See Ref. 20 for mode diagrams for these vibrations.) Although the $^+19^1m^x$ vibtor levels are mostly in the expected positions for *m*ClT$^+$ (see Table IV), both $^+19^1m^{3(+)}$ and $^+19^1m^4$ are significantly lower than expected, suggesting (currently unidentified) vibronic interactions in the cation for these levels.

We have calculated the torsional barrier in the *m*ClT$^+$ cation when we distort the geometry of the molecule along the D_{30} vibrational coordinate. Indeed, for small distortions along that coordinate, in line with that expected for the fundamental and first overtone levels, there is a lowering of the barrier by a few tens of cm^{-1}, in line with the experimental observations for both *m*FT$^+$ and *m*ClT$^+$.

V. CONCLUDING REMARKS

In the present work, we have recorded a significant number of ZEKE spectra via different S_1 torsional and vibtor levels, allowing confirmation of the assignment of the intermediate levels, and also obtaining both vibrational and torsional information on the cation. Further, as with *m*FT,[20] we have again found clear evidence for changes in torsional potentials, particularly involving the D_{30} vibration and its overtone, in the cation. Additionally, the anomalous intensity of the $^+30^1m^2$ band when exciting via m^1 and, more generally, the activity of $^+30^1m^x$ bands in the spectra for *m*FT and *m*ClT, confirm that certain out-of-plane vibrational motions are intricately linked to torsional motion. Overall, we conclude that it is unlikely that one can express the vibtor levels of $^+30^1$ and $^+30^2$ as simply products of torsional and vibrational wavefunctions.

The observation of activity for the out-of-plane 30^1 vibration in the $S_1 \leftarrow S_0$ transition is unexpected, since it is symmetry forbidden, and we have suggested that its activity here arises from a $m^4 \ldots 30^1 m^1$ interaction. It is interesting to note that the intensity of the $^+30^1 m^4$ band is much lower than might be expected, when exciting via the $30^1 m^1$ band, and similar anomalies were seen for m = 4 vibtor levels in ZEKE spectra via $30^1 m^4$ and $30^2 m^4$ levels in *m*FT.[20] We have also concluded that the $29^2 m^0$ and $29^2 m^1$ levels are not in the expected order, and hypothesised that there is a $29^1 m^5 \ldots 29^2 m^1$ interaction that caused the latter level to move up in wavenumber. We have also highlighted that the spacing between the $30^2 m^0$ and $30^2 m^1$ levels is greater than the expected 4 cm^{-1}, as seen for the origin bands and suggested various interactions.

We have also discussed the suggestion in Ref. 22 that there is an interaction between $^+m^5$ and $^+30^1 m^2$ (denoted b^1m^2 therein). This hypothesis was based upon the appearance of the ZEKE spectrum recorded via m^1 (see Figure 3) where, as well as the expected m^5 band, a very strong $^+30^1 m^2$ band is seen. However, we note that the $^+m^5$ band is in the expected position (see Table III) and, furthermore, that there is no such strong $^+30^1 m^2$ band when exciting via m^2 (Figure 3), with this being a shoulder on the side of the $^+m^5$ band in the spectrum seen when exciting via m^4 (Figure 3). Moreover, the $^+m^5$ band is not seen when exciting via $30^1 m^1$, while the $^+30^1 m^2$ band is relatively intense (Figure 4). While we concur that the $^+30^1$ vibration is interacting with the torsional motion, this is not a 1:1 interaction with a particular $^+m^x$ level, but a more general phenomenon, causing a change to the intermolecular potential. Clearly, the coupled motion of the $^+30^1$ vibration with the torsion is also leading to wavefunction changes that affect photoionization intensities unusually. With *m*FT,[20] we noted the surprisingly intense $^+30^1 m^4$ band, when exciting via m^4, and the intense $^+30^2 m^4$ band when exciting via $30^1 m^4$; on the other hand the $^+30^2 m^4$ band was anomalously weak when exciting via $30^2 m^1$. In the present work on *m*ClT, partly owing to overlapped bands, it is not possible to say definitively that these particular intensities are anomalous, although we do see prominent $^+30^1 m^x$ bands when exciting via m^4, for example.

We now comment on the V_3 barriers in the S_0, S_1 and D_0^+ states. By reference to the geometries of *m*FT in these three states[20] and Figure 9 for *m*ClT, there is not the marked asymmetry in the C-C bond lengths in the S_1 state that there are in the D_0^+ state. Thus, the explanation of the significantly larger barrier in the S_1 state cannot be solely attributed to asymmetric charge distributions, as suggested by Feldgus et al.[22] On the other hand, there is a reasonably significant shortening of the C-CH_3 bond length, $S_1 \leftarrow S_0$, which would increase the "vdW" interaction with the "ortho" hydrogens, and this would be a plausible explanation of the increase in barrier height. For $D_0^+ \leftarrow S_1$ the C-CH_3 bond length is about the same in the two states, but now we have the asymmetry in charge distribution (see next paragraph and Refs. 20 and 22), and this both increases the barrier, and switches the equilibrium geometry from *pseudo*-trans (for S_0 and S_1) to *pseud*o-cis (for D_0^+).

Also, in agreement with Feldgus et al.,[22] we find that the main V_3 torsional barrier in *m*ClT is slightly lower than in *m*FT. This barrier appears to be associated with an asymmetry in the charge distribution in the carbon-

carbon bonds closest to the C-CH_3 bond, indicated by the C-C bond lengths (see Figure 9), and has been discussed by Weisshaar's group[22,32] and ourselves.[20] This asymmetry is largely due to the electron density distribution of the highest occupied molecular orbital (HOMO) of the S_0 state of the substituted benzene, which has electron density concentrated in two C-C bonds on opposite sides of the benzene ring, adjacent to each of the substituents. Once the molecule is ionized, this leads to two regions of more-concentrated positive charge in these positions. Further modifications of the electron density occur depending on the substituents, such as their electronegativity. Hence, the lower barrier for the less electronegative Cl substituent makes sense, since it can tolerate the neighbouring positive charge better than can the more electronegative F atom. This difference is contained in the difference in the C-C bond lengths either side of the methyl substituent, which Feldgus et al.[22] have noted is related to the difference in the natural bond order. For *m*FT, the difference is 0.072 Å, while in *m*ClT it is 0.063 Å, in line with the somewhat smaller V_3 barrier for *m*ClT. Further, the removal of the electron is expected to be easier for *m*ClT than *m*FT, and this is in line with the lower AIE for *m*ClT (71319 cm^{-1}) than for *m*FT (71997 cm^{-1}).[20]

Lastly, we note that the high barrier in the D_0^+ state suggests that the lower torsional levels are close to being vibrational levels. This would mean the rotor motion is significantly localized and would suggest that the methyl group C-H bonds would not all be of equal lengths. Under these circumstances, as suggested for *m*FT,[20] there would be a movement away from molecular group symmetry, towards point group symmetry.

We note that other explanations for barrier height variation have been put forward, including π^*/σ^* interactions that underlie hyperconjugation.[33,34] The idea is that variations in orbital energies suggest that the LUMO is the key factor in determining barrier heights, and correlations with the Hammett constant suggested. However, we note that this explanation has been challenged by Suzuki et al.[35] and does not seem to explain the high barriers in the cation, where the orbital corresponding to the LUMO of the neutral molecule is unoccupied; thus, for the cation, we prefer the explanations of Weisshaar and coworkers, discussed in the present work. We also note that barriers for molecules such as toluene and *p*FT the barrier will be a V_6 term, while for *ortho* and *meta* molecules, the barriers will be V_3 terms; further determining such barriers directly from spectra can be problematic because of vibtor interactions, as discussed herein, and reliable determination of barrier heights from quantum chemistry likely requires a more-systematic study of electron correlation effects and basis set requirements.

The *m*FT and *m*ClT molecules represent very interesting molecules owing to the very different barrier heights in the three electronic states studied. In particular, this provides access to a significant number of torsional and vibtor levels in the cation. This has provided fruitful ground for investigating the interactions between torsional and vibrational motion, which is widely accepted as being a key aspect of internal energy flow and changes in photophysical behaviour.

Acknowledgements

We are grateful to the EPSRC for funding (grant EP/L021366/1). The EPSRC and the University of Nottingham are thanked for a studentship to D.J.K. L.G.W. is grateful for an Undergraduate Summer Bursary funded via a University of Nottingham School of Chemistry 1960 scholarship. We are grateful for continued discussions with Warren Lawrance and Jason Gascooke (Flinders, Adelaide) regarding vibration-torsion interactions.

Table I: Calculated and experimental vibrational wavenumbers (cm^{-1}) for *m*ClT in the S_0, S_1 and D_0^+ states[a]

D_i[b]	S_0		S_1		D_0^+	
	Calculated	Experiment	Calculated	Experiment	Calculated	Experiment
			a_1			
D_1	3109	3085	3127		3119	
D_2	3089	3064	3113		3109	
D_3	3087		3122		3110	
D_4	3071		3080		3089	
D_5	1562	1578	1489		1539	
D_6	1588	1604	1473		1370	
D_7	1468	1478	1391		1429	
D_8	1404	1467	1337		1354	
D_9	1298	1296	1259		1340	
D_{10}	1194	1221	1187		1203	
D_{11}	1270	1272	1403		1263	
D_{12}	1155	1164	1127		1121	
D_{13}	1069	1096	1013		1059	
D_{14}	1086	1079	1038		1082	
D_{15}	989	1002	955	[962][c]	983	
D_{16}	835	858 [865][c]	817	[823][c]	840	
D_{17}	675	684 [687][c]	636	[635][c]	665	
D_{18}	513	522 [524][c]	446	[454][c]	455	457[d]
D_{19}	402	416 [409][c]	373	[374][c]	391	396[d]
D_{20}	376	387 [387][c]	368		377	
D_{21}	226	221	226	231[d]	233	240[d]
			a_2			
D_{22}	970	976	782		991	
D_{23}	894	898	714		926	
D_{24}	871	869	535		863	
D_{25}	770	776	584		781	
D_{26}	683	684	468		589	
D_{27}	526	522	376		495	
D_{28}	432	431	241		366	
D_{29}	213	234	159	151[d]	176	176[d]
D_{30}	171	185	80	107[d]	150	149[d]

[a] Frequencies calculated at the optimized geometries. For the S_0 state, the level of calculation was B3LYP/aug-cc-pVTZ (values very similar to those in Ref. 24); for the S_1 state, TD-B3LYP/aug-cc-pVTZ; and for the D_0^+ state, UB3LYP/aug-cc-pVTZ. In all cases, the calculated harmonic vibrational wavenumbers were scaled by 0.97. Values reported are for the ^{35}Cl isotopologue.

[b] The D_i labels are described in Ref. 24, where the vibration mode diagrams can also be found.

[c] Values taken from the fluorescence study of Ichimura et al.[21]

[d] Present work. The S_1 values for D_{29} and D_{30} are estimated from the respective overtone bands.

Table II: Correspondence of the C_s point group symmetry classes with those of the G_6 molecular symmetry group. Also indicated are the symmetries of the D_i vibrations and the different pure torsional levels.[a]

C_s	G_6	D_i[b]	m
a'	a_1	D_1–D_{21}	0, 3(+),6(+), 9(+)
a''	a_2	D_{21}–D_{30}	3(-),6(-), 9(-)
	e		1,2,4,5,7,8

[a] Symmetries of vibtor levels can be obtained by combining the vibrational symmetry (in G_6) with those of the pure torsional level, using the C_{3v} point group direct product table.

[b] The D_i labels are described in Ref. 24, where the vibration mode diagrams can also be found.

Table III

m	S_1		D_0^+	
	Calculated	Observed	Calculated	Observed
0	0	0	0	0
1	0.79	1	0.1	0
2	48.2	48	96.4	98
3(-)	56.3	56	97.7	98
3(+)	86.2	88	177.2	175
4	107.5	106	186.9	186
5	150.6		246.0	246
6(-)	203.2		286.9	284
6(+)	204.8		301.1	300
7	268.3		359.8	363
8	342.8		437.8	439
9(-)	427.5		530.9	
9(+)	427.5		531.1	

S_1 V_3 = 110 cm^{-1}; V_6 = -20 cm^{-1}; F = 5.0 cm^{-1}.

D_0^+ V_3 = 287.5 cm^{-1}; V_6 = -20 cm^{-1}; F = 5.4 cm^{-1}.

Table IV: Separations of vibtor levels built on different vibrations (cm^{-1}).[a]

	Vibrational Level[b]							
Torsion[c]	$^{+}0^{0}$ [0]	$^{+}30^{1}$ [149]	$^{+}29^{1}$ [176]	$^{+}21^{1}$ [240]	$^{+}30^{2}$ [294]	$^{+}29^{2}$ [354]	$^{+}19^{1}$ [396]	$^{+}18^{1}$ [456]
$^{+}m^{0,1}$	0	0	0	0	0	0	0	0
$^{+}m^{2}$	98	89 (238)	101 (277)	99 (339)	87 (381)	94 (448)	90 (486)	97 (555)
$^{+}m^{3(-)}$	98	89 (238)	98 (273)					
$^{+}m^{3(+)}$	175			176 (416)	172 (466)	175 (529)	167 (563)	177 (633)
$^{+}m^{4}$	186	173 (322)	182 (358)	187 (427)	168 (462)	184 (538)	177 (573)	186 (642)
$^{+}m^{5}$	246	230 (379)	240 (416)	239 (479)	229 (523)	247 (601)	246 (642)	248 (704)
$^{+}m^{6(-)}$	284						272 (668)	278 (734)
$^{+}m^{6(+)}$	300			307 (547)	286 (580)	298 (652)	295 (691)	300 (756)
$^{+}m^{7}$	363							
$^{+}m^{8}$	439							

[a] Torsional spacings are given with respect to the band position of the $^{+}m = 0$ or $^{+}m^{1}$ level of the indicated vibration.

[b] Values in square brackets in the column headers are the wavenumbers of the $^{+}m = 0$ level of the indicated vibration. Values in parentheses are the vibtor band positions, while the values outside parentheses are the spacings between the vibtor levels for the particular vibration. For weak bands and overlapped features, we have given our best estimate of the band position.

[c] The $^{+}m^{0}$ and $^{+}m^{1}$ levels are degenerate at our resolution (see Table 3). Levels with $^{+}m \neq 3n$ have degenerate + and – levels.

Figure Captions

Figure 1: Comparison between the 0–350 cm^{-1} regions above the origins of the $S_1 \leftarrow S_0$ transitions in *m*-chlorotoluene and *m*-fluorotoluene. The assignments for the latter have been discussed in Refs. 19 and 20, and there is a high degree of consistency between the two sets of spectra. The asterisked bands are thought to arise from complexes. See text for further discussion of the assignments.

Figure 2: ZEKE spectra recorded via two a_1 symmetry torsional levels of the S_1 state. The preceding superscripted "+" used in the text is omitted in the labels for clarity. See text for further discussion of the assignments.

Figure 3: ZEKE spectra recorded via three *e* symmetry torsional levels of the S_1 state. The preceding superscripted "+" used in the text is omitted in the labels for clarity. See text for further discussion of the assignments.

Figure 4: ZEKE spectra recorded via vibtor levels of the S_1 state involving the 30^1 vibration; the ZEKE spectrum via m^4 is shown for comparison. It is concluded that there are two overlapped transitions at the excitation energy used for the third trace; comparison is made here for the 30^1m^4 contribution, with the 30^2m^1 contributions being highlighted in Figure 6. The preceding superscripted "+" used in the text is omitted in the labels for clarity. See text for further discussion of the assignments.

Figure 5: ZEKE spectrum recorded via the $29^1m^{3(-)}$/ 29^1m^2 overlapped transitions of the S_1 state. The preceding superscripted "+" used in the text is omitted in the labels for clarity. Note that bands arising from transitions involving *e* symmetry bands are actually 4 cm^{-1} higher than indicated on the scale in this particular spectrum. See text for further discussion of the assignments.

Figure 6: ZEKE spectra recorded via the 30^2m^0 and 30^2m^1 levels of the S_1 state. In the latter case, the transition is overlapped with the 30^1m^4 level. The preceding superscripted "+" used in the text is omitted in the labels for clarity. See text for further discussion of the assignments, and also Figure 4.

Figure 7: ZEKE spectra recorded via the 21^1m^0 and 21^1m^1 levels of the S_1 state. The preceding superscripted "+" used in the text is omitted in the labels for clarity. See text for further discussion of the assignments.

Figure 8: In the top trace, an expanded via of the 270–320 cm^{-1} region of the REMPI spectrum of the $S_1 \leftarrow S_0$ transition of *m*-chlorotoluene is shown. Below this are ZEKE spectra recorded via the 29^2m^0 and 29^2m^1 levels of the S_1 state. In the case of the latter, there is some evidence for an interaction with the 29^1m^5 state. See text for further discussion of the assignments.

Figure 9: Calculated geometries for the (a) S_0 (B3LYP/aug-cc-pVTZ), (b) S_1(TD-B3LYP/aug-cc-pVTZ), and (c) D_0^+ (UB3LYP/aug-cc-pVTZ) electronic states of *m*-chlorotoluene. The bond lengths are in Å. Note the differing conformation of the cation relative to the two neutral states. The filled circle represents the Cl atom, the C and H atoms are both unfilled circles.

Figure 1

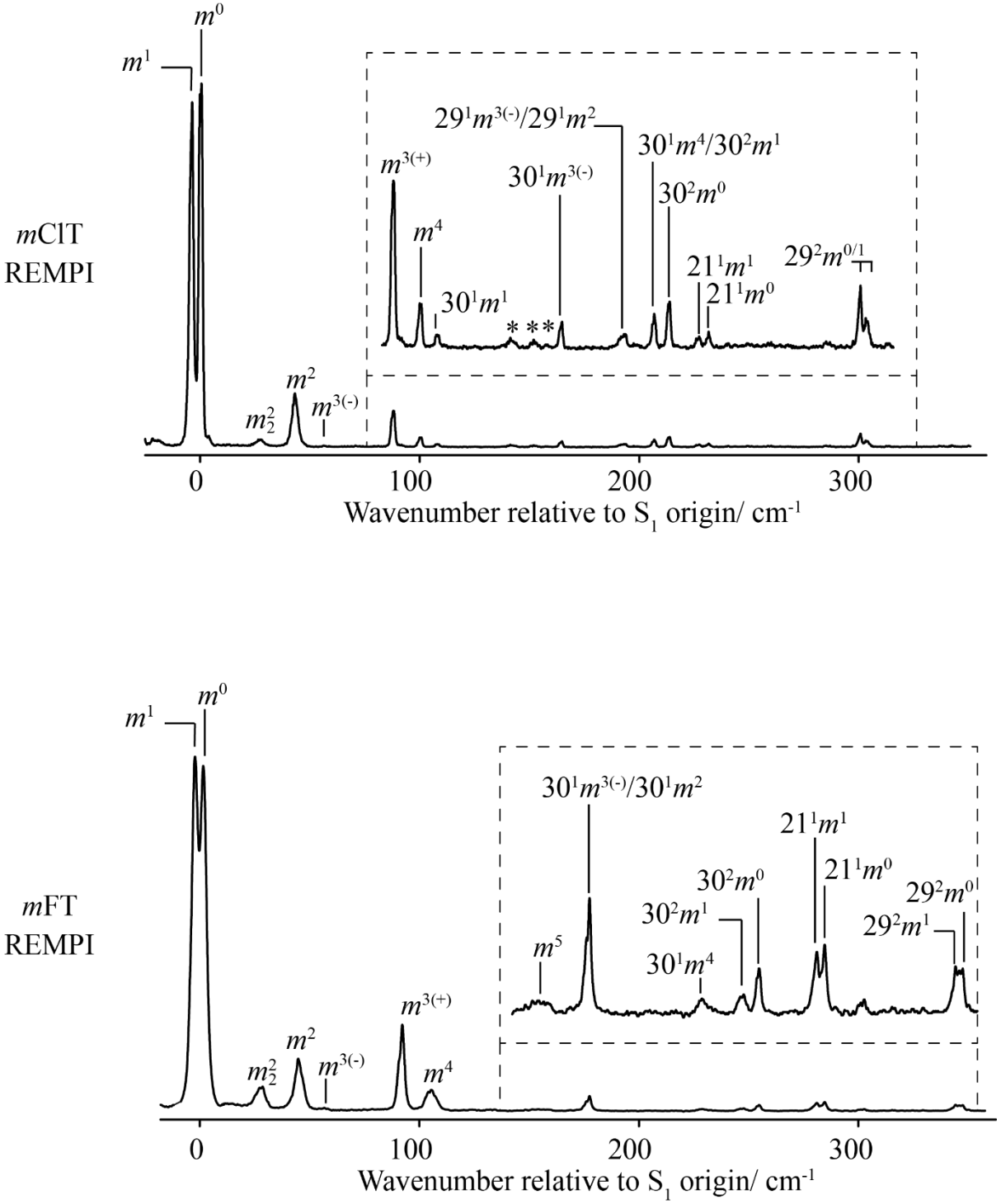
mClT
REMPI
m0
m1
29¹m3(-)/29¹m2
30¹m4/30²m1
m3(+)
30¹m3(-)
30²m0
m4
29²m0/1
21¹m1
21¹m0
30¹m1
* * *
m2
m2²
m3(-)
0
100
200
300
Wavenumber relative to S1 origin/ cm-1
mFT
REMPI
m0
m1
30¹m3(-)/30¹m2
21¹m1
21¹m0
30²m0
29²m0
30²m1
29²m1
m5
30¹m4
m3(+)
m2
m2²
m3(-)
m4
0
100
200
300
Wavenumber relative to S1 origin/ cm-1

Figure 2

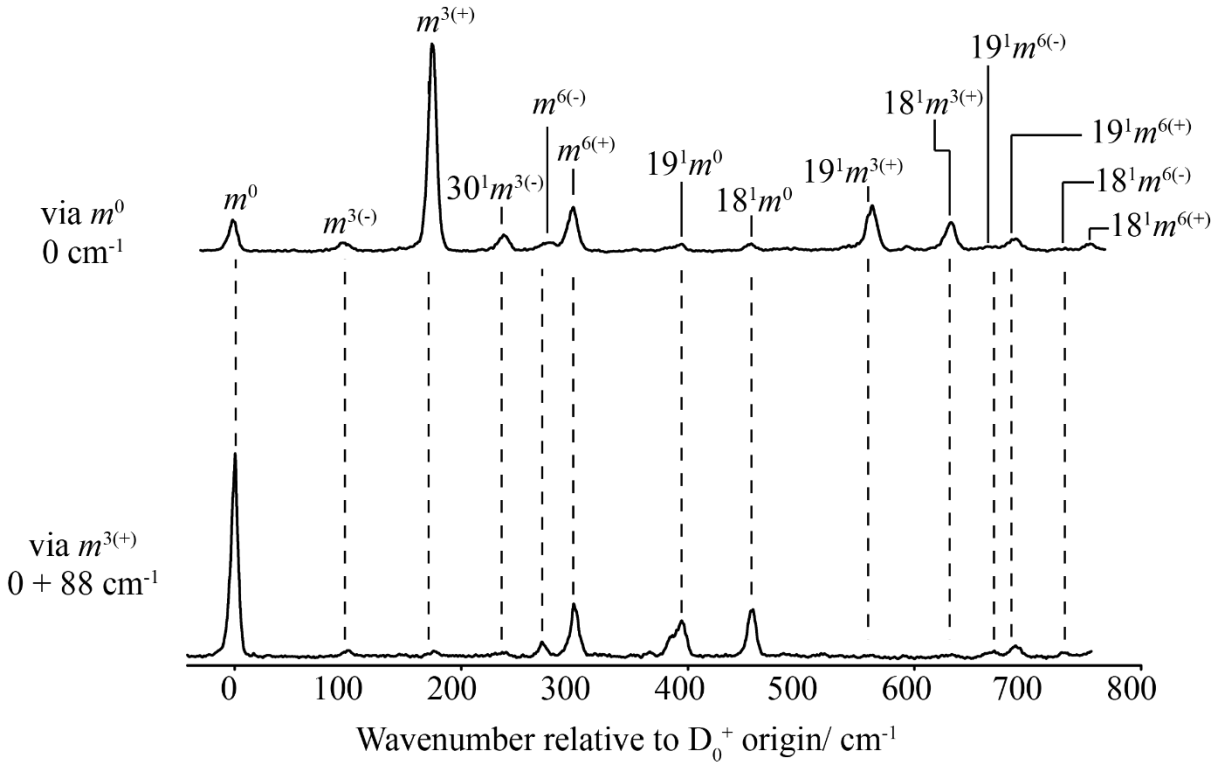
$m^{3(+)}$
$19^1m^{6(-)}$
$m^{6(-)}$
$18^1m^{3(+)}$
$19^1m^{6(+)}$
$m^{6(+)}$
19^1m^0
$19^1m^{3(+)}$
$18^1m^{6(-)}$
m^0
$30^1m^{3(-)}$
18^1m^0
$18^1m^{6(+)}$
$m^{3(-)}$
via m^0
0 cm^{-1}
via $m^{3(+)}$
0 + 88 cm^{-1}
0
100
200
300
400
500
600
700
800
Wavenumber relative to D_0^+ origin/ cm^{-1}

Figure 3

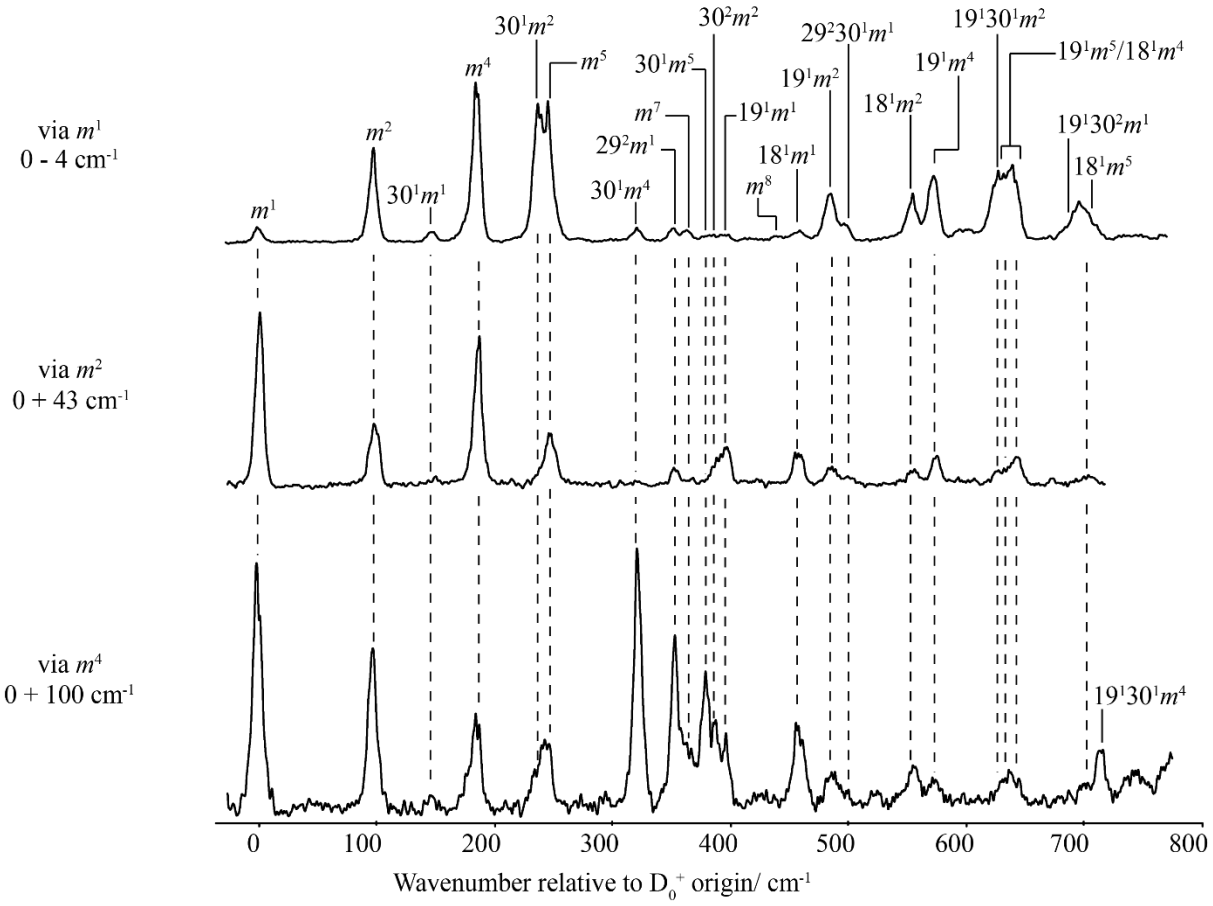
via m^1
0 - 4 cm^{-1}
via m^2
0 + 43 cm^{-1}
via m^4
0 + 100 cm^{-1}
m^1
m^2
30^1m^1
m^4
30^1m^2
m^5
30^1m^4
29^2m^1
m^7
30^1m^5
30^2m^2
m^8
19^1m^1
18^1m^1
$29^230^1m^1$
19^1m^2
18^1m^2
19^1m^4
$19^130^1m^2$
$19^1m^5/18^1m^4$
$19^130^2m^1$
18^1m^5
$19^130^1m^4$
0
100
200
300
400
500
600
700
800
Wavenumber relative to D_0^+ origin/ cm^{-1}

Figure 4

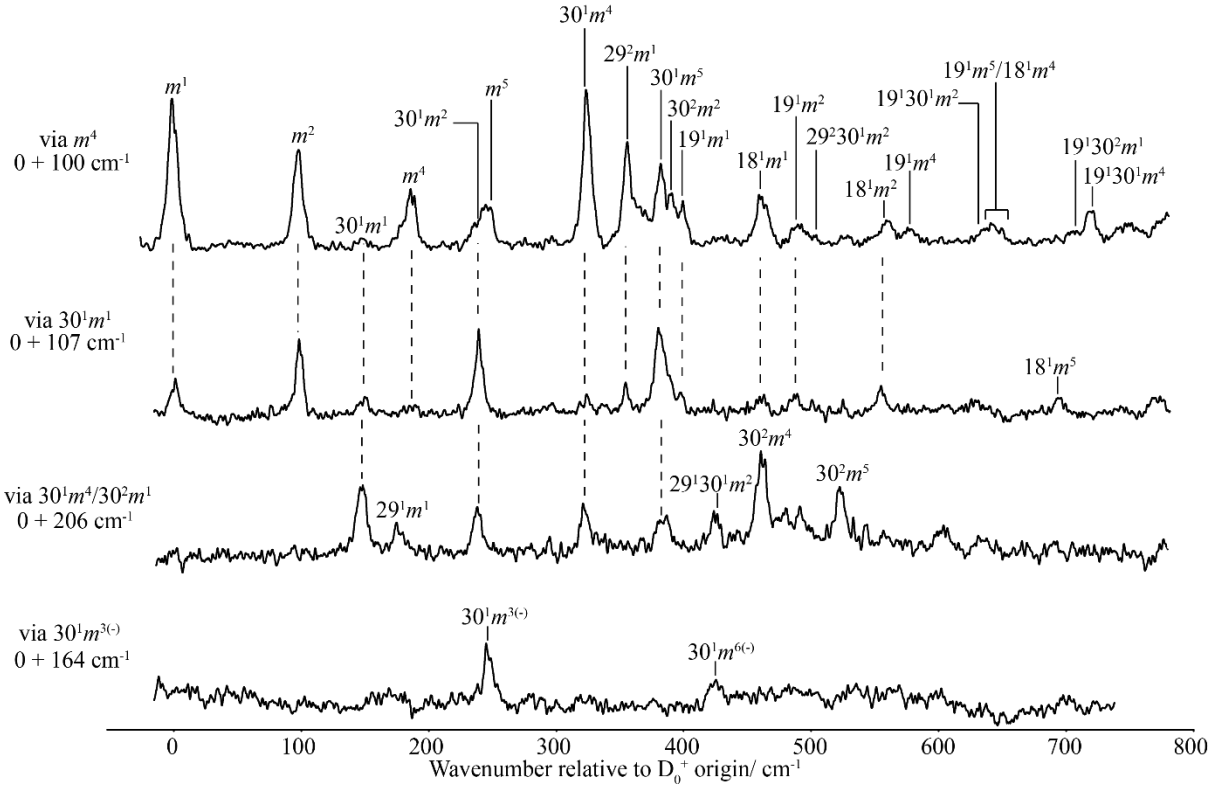
via m^4
0 + 100 cm^{-1}
via 30^1m^1
0 + 107 cm^{-1}
via $30^1m^4/30^2m^1$
0 + 206 cm^{-1}
via $30^1m^{3(-)}$
0 + 164 cm^{-1}
m^1
m^2
30^1m^1
m^4
30^1m^2
m^5
30^1m^4
29^2m^1
30^1m^5
30^2m^2
19^1m^1
18^1m^1
19^1m^2
$29^230^1m^2$
18^1m^2
19^1m^4
$19^130^1m^2$
$19^1m^5/18^1m^4$
$19^130^2m^1$
$19^130^1m^4$
18^1m^5
29^1m^1
30^2m^4
$29^130^1m^2$
30^2m^5
$30^1m^{3(-)}$
$30^1m^{6(-)}$
0
100
200
300
400
500
600
700
800
Wavenumber relative to D_0^+ origin/ cm^{-1}

Figure 5

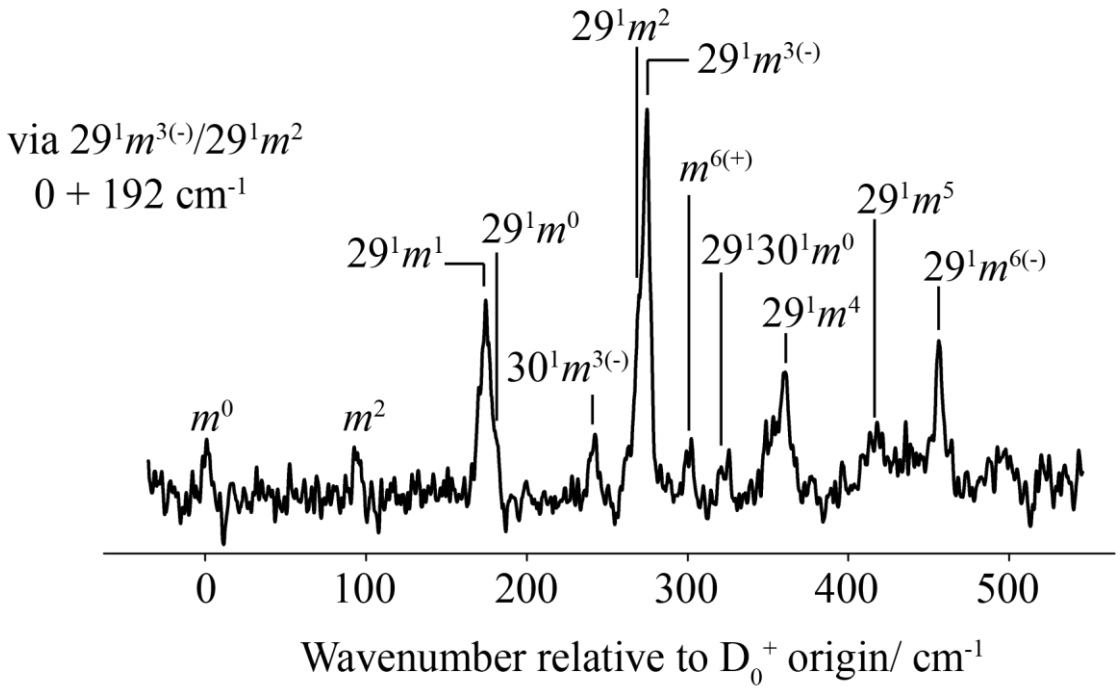
via $29^1m^{3(-)}/29^1m^2$
0 + 192 cm^{-1}
29^1m^2
$29^1m^{3(-)}$
$m^{6(+)}$
29^1m^5
29^1m^1
29^1m^0
$29^130^1m^0$
$29^1m^{6(-)}$
29^1m^4
$30^1m^{3(-)}$
m^0
m^2
0
100
200
300
400
500
Wavenumber relative to D_0^+ origin/ cm^{-1}

Figure 6

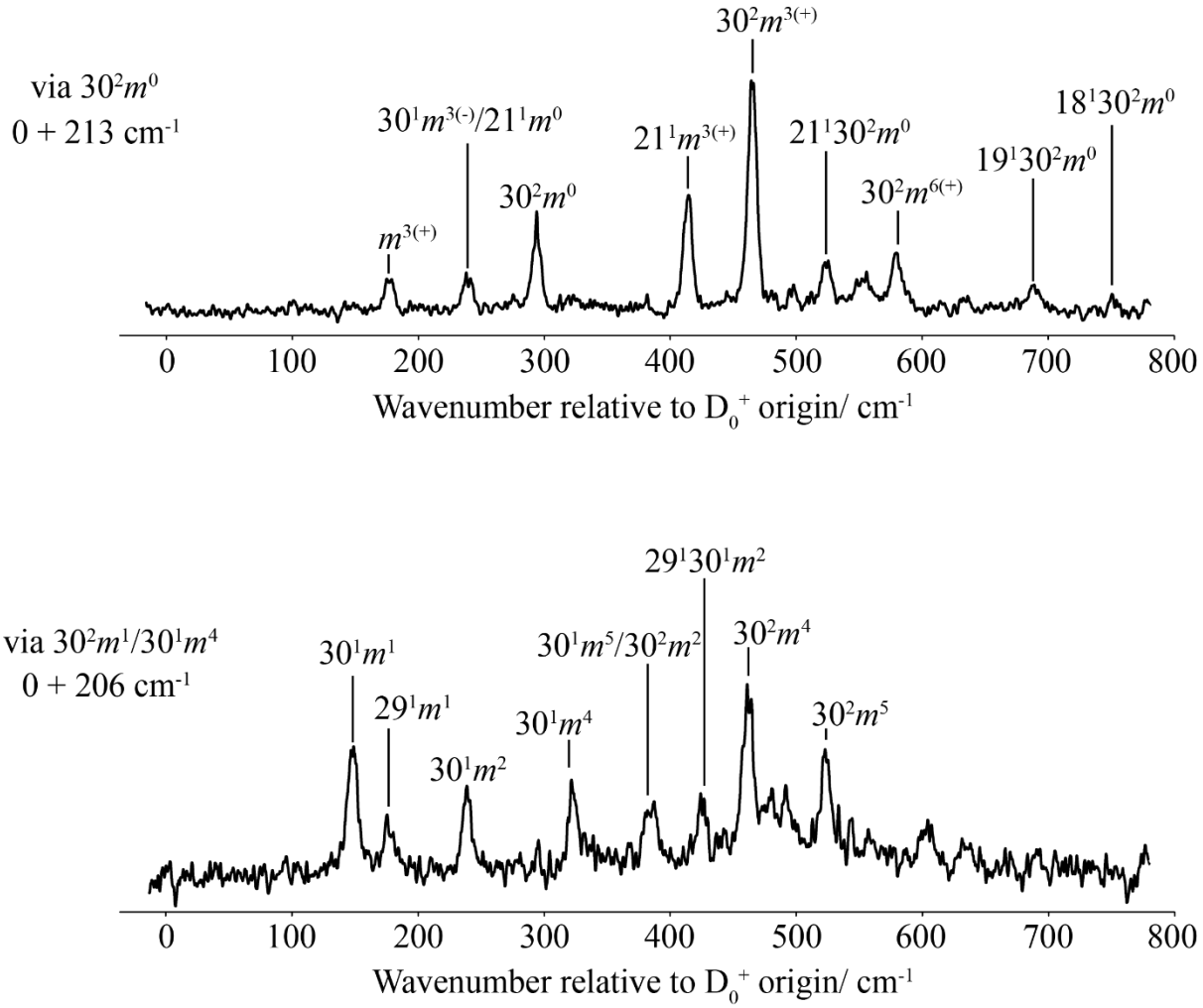
via 30^2m^0
0 + 213 cm^{-1}
$30^2m^{3(+)}$
$30^1m^{3(-)}/21^1m^0$
$21^1m^{3(+)}$
$21^130^2m^0$
$18^130^2m^0$
$19^130^2m^0$
$30^2m^{6(+)}$
30^2m^0
$m^{3(+)}$
0
100
200
300
400
500
600
700
800
Wavenumber relative to D_0^+ origin/ cm^{-1}
via $30^2m^1/30^1m^4$
0 + 206 cm^{-1}
$29^130^1m^2$
30^1m^1
$30^1m^5/30^2m^2$
30^2m^4
29^1m^1
30^1m^4
30^2m^5
30^1m^2
0
100
200
300
400
500
600
700
800
Wavenumber relative to D_0^+ origin/ cm^{-1}

Figure 7

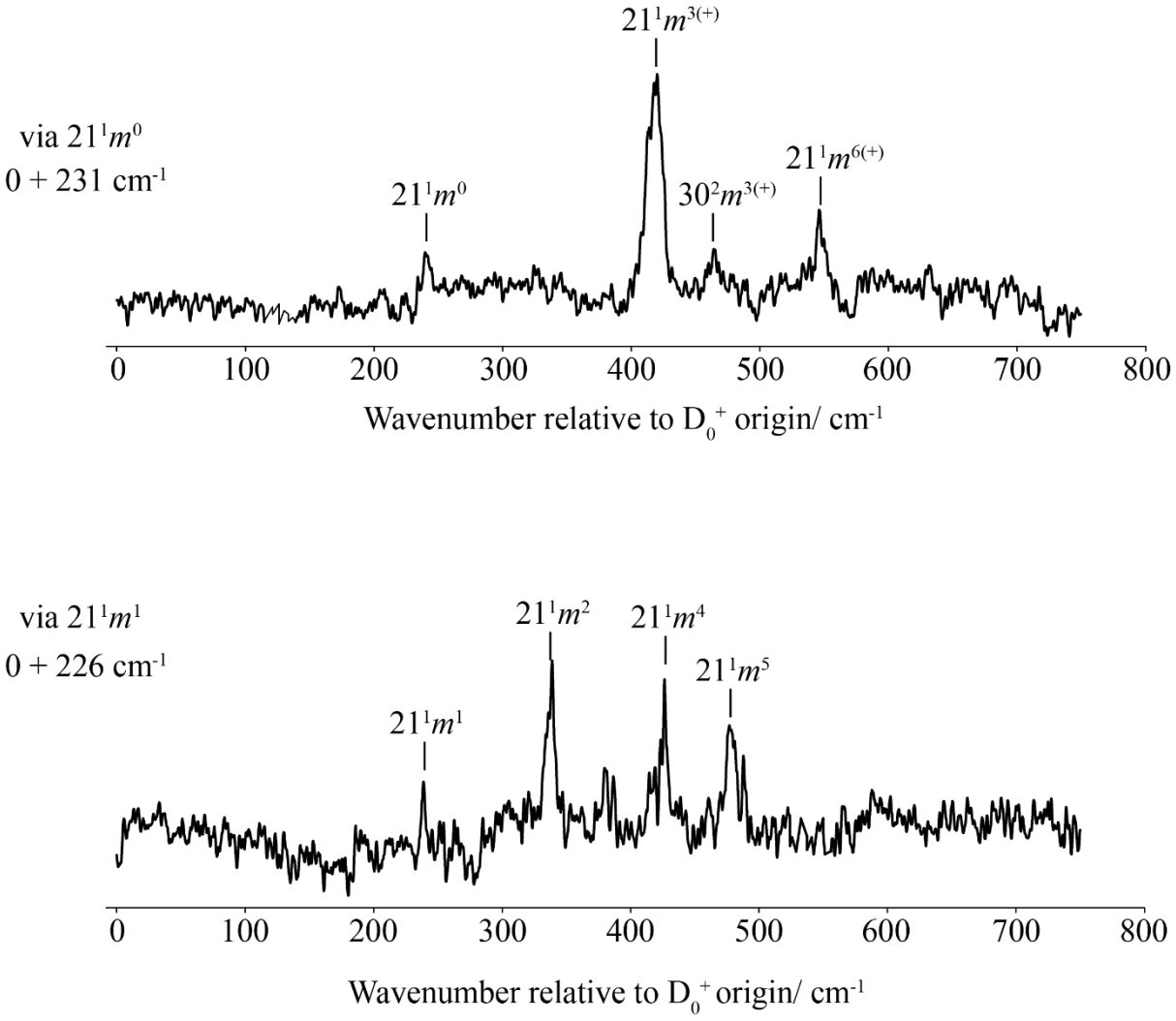
via 21^1m^0
0 + 231 cm^{-1}
$21^1m^{3(+)}$
21^1m^0
$30^2m^{3(+)}$
$21^1m^{6(+)}$
0
100
200
300
400
500
600
700
800
Wavenumber relative to D_0^+ origin/ cm^{-1}
via 21^1m^1
0 + 226 cm^{-1}
21^1m^2
21^1m^4
21^1m^5
21^1m^1
0
100
200
300
400
500
600
700
800
Wavenumber relative to D_0^+ origin/ cm^{-1}

Figure 8

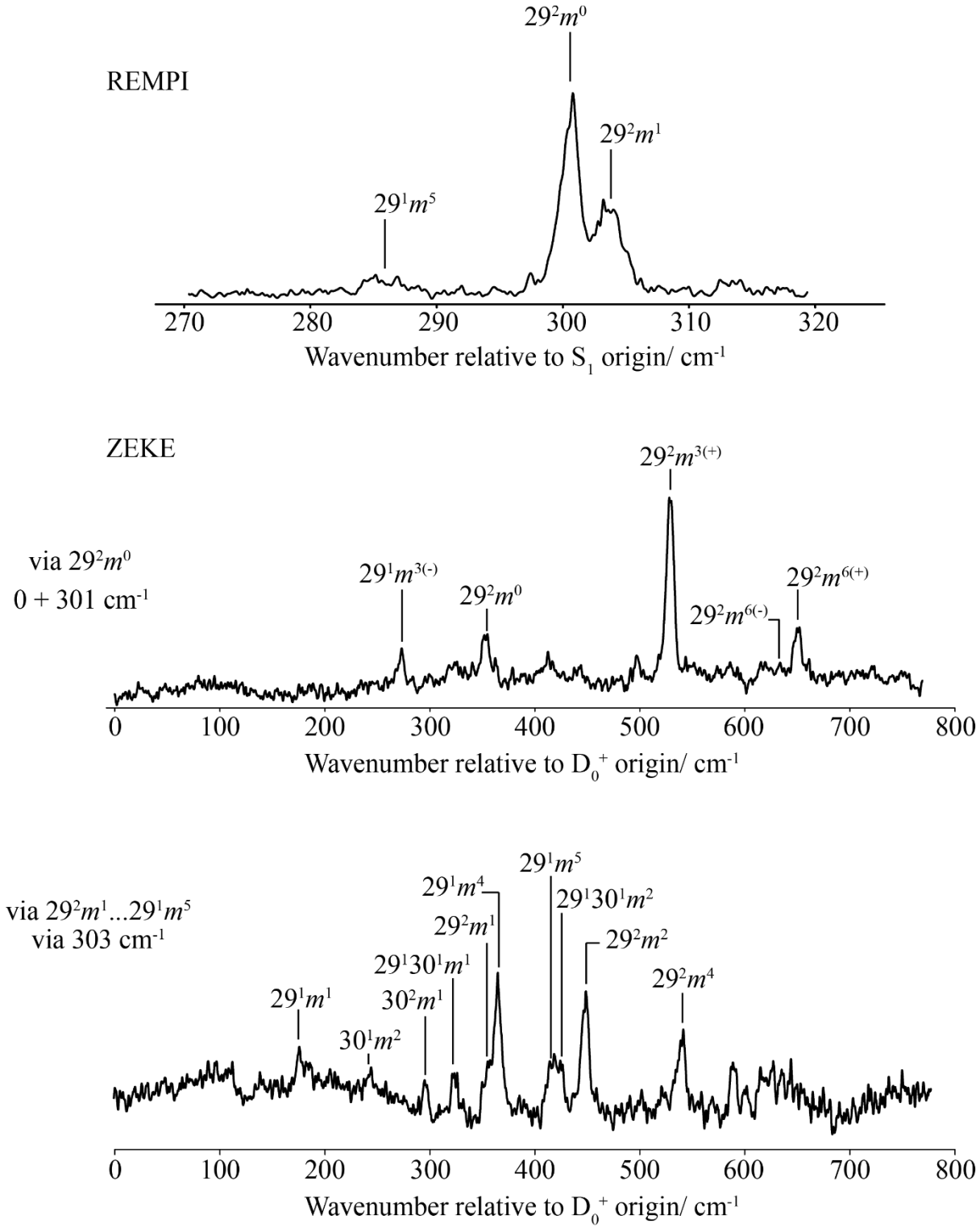
REMPI
29^2m^0
29^2m^1
29^1m^5
270
280
290
300
310
320
Wavenumber relative to S_1 origin/ cm^{-1}
ZEKE
via 29^2m^0
0 + 301 cm^{-1}
$29^2m^{3(+)}$
$29^1m^{3(-)}$
29^2m^0
$29^2m^{6(-)}$
$29^2m^{6(+)}$
0
100
200
300
400
500
600
700
800
Wavenumber relative to D_0^+ origin/ cm^{-1}
via $29^2m^1...29^1m^5$
via 303 cm^{-1}
29^1m^5
29^1m^4
$29^130^1m^2$
29^2m^1
29^2m^2
$29^130^1m^1$
29^2m^4
29^1m^1
30^2m^1
30^1m^2
0
100
200
300
400
500
600
700
800
Wavenumber relative to D_0^+ origin/ cm^{-1}

Figure 9

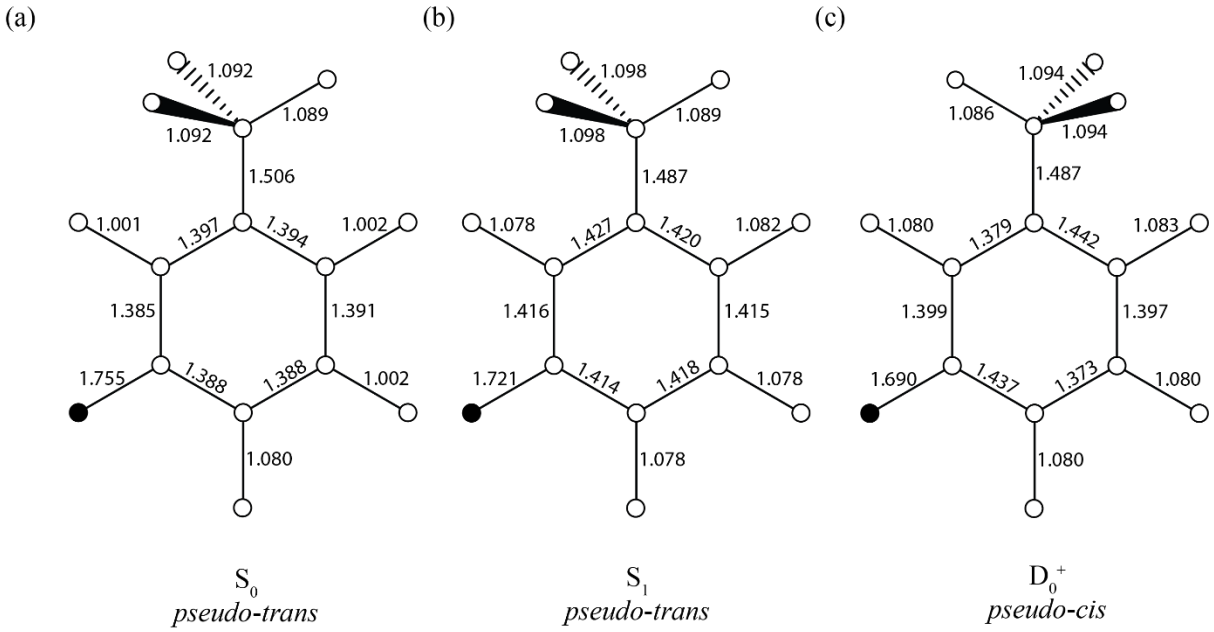
(a)
(b)
(c)
1.092
1.089
1.092
1.506
1.001
1.397
1.394
1.002
1.385
1.391
1.755
1.388
1.388
1.002
1.080
1.098
1.089
1.098
1.487
1.078
1.427
1.420
1.082
1.416
1.415
1.721
1.414
1.418
1.078
1.078
1.094
1.086
1.094
1.487
1.080
1.379
1.442
1.083
1.399
1.397
1.690
1.437
1.373
1.080
1.080
S0
pseudo-trans
S1
pseudo-trans
D0+
pseudo-cis

References

[1] R. Improta, F. Santoro, and L. Blancafort, Chem. Rev. **116**, 3540 (2016).

[2] R. Barata-Morgado, M. L. Sanchez, A. Munoz-Losa, M. E. Martin, F. J.O. del Valle, and M. Aguilar, J. Phys. Chem. A **122**, 3096 (2018).

[3] Y. K. Kosenkov and D. Kosenkov, J. Chem. Phys. **151**, 144101 (2019).

[4] J. A. Davies, A. M. Green, A. M. Gardner, C. D. Withers, T. G. Wright, and K. L. Reid, Phys. Chem. Chem. Phys. **16**, 430 (2014).

[5] A. M. Gardner, A. M. Green, V. M. Tamé-Reyes, V. H. K. Wilton, and T. G. Wright, J. Chem. Phys. **138**, 134303 (2013).

[6] J. R. Gascooke, E. A. Virgo, and W. D. Lawrance, J. Chem. Phys. **143**, 044313 (2015).

[7] A. M. Gardner, W. D. Tuttle, L. Whalley, A. Claydon, J. H. Carter, and T. G. Wright, J. Chem. Phys. **145**, 124307 (2016).

[8] J. R. Gascooke, L. D. Stewart, P. G. Sibley, and W. D. Lawrance, J. Chem. Phys. **149**, 074301 (2018).

[9] A. M. Gardner, W. D. Tuttle, L. E. Whalley, and T. G. Wright, Chem. Sci. **9**, 2270 (2018).

[10] W. D. Tuttle, A. M. Gardner, L. E. Whalley, D. J. Kemp, and T. G. Wright, Phys. Chem. Chem. Phys. **21**, 14133 (2019).

[11] D. J. Kemp, A. M. Gardner, W. D. Tuttle, and T. G. Wright, Molec. Phys. **117**, 3011 (2019).

[12] D. J. Kemp, W. D. Tuttle, A. M. Gardner, L. E. Whalley, and T. G. Wright, J. Chem. Phys. **151**, 064308 (2019).

[13] J. A. Davies, L. E. Whalley and K. L. Reid, Phys. Chem. Chem. Phys. **19**, 5051 (2017).

[14] A. M. Gardner, L. E. Whalley, D. J. Kemp, W. D. Tuttle and T. G. Wright, J. Chem. Phys. **151**, 154302 (2019).

[15] A. M. Gardner, L. E. Whalley, D. J. Kemp, W. D. Tuttle, and T. G. Wright, **151**, 154302 (2019).

[16] A. M. Gardner, W. D. Tuttle, P. Groner, and T. G. Wright, J. Chem. Phys. **146**, 124308 (2017).

[17] W. D. Tuttle, A. M. Gardner, K. B. O'Regan, W. Malewicz, and T. G. Wright, J. Chem. Phys. **146**, 124309 (2017).

[18] P. J. Timbers, C. S. Parmenter, and D. B. Moss, J. Chem. Phys. **100**, 1028 (1994).

[19] L. D. Stewart, J. R. Gascooke, and W. D. Lawrance, J. Chem. Phys. **150**, 174303 (2019).

[20] D. J. Kemp, E. F. Fryer, A. R. Davies, and T. G. Wright, J. Chem. Phys. **151**, 084311 (2019).

[21] T. Ichimura, A. Kawana, T. Suzuki, T. Ebata, and N. Mikami, J. Photochem. Photobiol. A: Chem. **80**, 145 (1994).

[22] S. H. Feldgus, M. J. Schroeder, R. A. Walker, W.-K. Woo, and J. C. Weisshaar, Int. J. Mass Spectrom. Ion. Proc. **159**, 231 (1996).

[23] V. L. Ayles, C. J. Hammond, D. E. Bergeron, O. J. Richards, and T. G. Wright, J. Chem. Phys. **126**, 244304 (2007).

[24] D. J. Kemp, W. D. Tuttle, F. M. S. Jones. A. M. Gardner, A. Andrejeva, J. C. A. Wakefield, and T. G. Wright, J Mol. Spect. **346**, 46 (2018).

[25] E. Fermi, Z. Phys. **71**, 250 (1931).

[26] J. R. Gascooke and W. D. Lawrance, J. Chem. Phys. **138**, 134302 (2013).

[27] N. T. Whetton and W. D. Lawrance, J. Phys. Chem. **93**, 5377 (1989).

[28] L. H. Spangler, Annu. Rev. Phys. Chem. **48**, 481 (1997).

[29] R. D. Gordon and J. M. Hollas, Chem. Phys. Lett. **164**, 255 (1989).

[30] J. D. Lewis, T. B. Malloy, Jr., T. H. Chao, and J. Laane, J. Molec. Struct. **12**, 427 (1972).

[31] X. Zhang, J. M. Smith, and J. L. Knee, J. Chem. Phys. **97**, 2843 (1992).

[32] K.-T. Lu, F. Weinhold, and J. C. Weisshaar, J. Chem. Phys. **102**, 6787 (1995).

[33] H. Nakai and M. Kawai, Chem. Phys. Lett. **307**, 272 (1999).

[34] H. Nakai and M. Kawai, J. Chem. Phys. **113**, 2168 (2000).

[35] K. Suzuki, S.-I. Ishiuchi, M. Sakai, and M. Fujii, J. Electron. Spectrosc. Rel. Phenom. **142**, 215 (2005).